Solar Combined Cycle with high-temperature Thermochemical Energy Storage

C. Ortiz [a,*], C. Tejada [bc], R. Chacartegui [b], R. Bravo [d], A. Carro [b], J.M. Valverde [e], J. Valverde [cf]

[a] Materials and Sustainability Group, Department of Engineering, Universidad Loyola Andalucía, Avda. de las Universidades s/n, 41704 Dos Hermanas, Seville, Spain

[b] Dpto. Ingeniería Energética. Universidad de Sevilla, Camino de los Descubrimientos s/n, 41092 Sevilla, Spain

[c] VirtualMechanics, S.L., c/ Arquitectura 1, 41015 Sevilla, Spain

[d] Department of Electrical and Electronic Engineering, The University of Manchester, School of Engineering, Institute for Energy Systems, The University of Edinburgh, UK

[e] Dpto. Electrónica y Elecromagnetismo, Universidad de Sevilla, Avenida Reina Mercedes s/n, 41012 Sevilla, Spain

[f] Dpto. de Matemática Aplicada 2. Universidad de Sevilla, Camino de los Descubrimientos s/n, 41092 Sevilla, Spain

[*] Corresponding author: cortiz@uloyola.es (+34) 655783930

Abstract

The present work proposes integrating a high-temperature thermochemical energy storage cycle to boost the solar contribution in solar combined cycles. The main feature of the plant is the possibility of storing solar energy at a very high temperature and releasing it on demand to drive the combined cycle in the absence of solar radiation. Based on the reversible calcination-carbonation of CaCO3/CaO, the Calcium-looping process is proposed since it allows power production above 900ºC by using cheap, non-toxic and widely available raw materials (i.e. limestone or dolomite). Based on an air-open and a CO2-closed combined cycle, two potential configurations are modelled and analysed, including designing a 360º solar field with a 200-meter tower. The novel solar combined cycle analyzed in the present work enhances the annual solar share above 50%, whilst the current state-of-the-art technology is below 15%. From actual solar irradiation data and clustering analysis, results show overall plant efficiencies over 45% (considering off-design performance) with a very high dispatchability, which justifies the interest in further developing this novel cycle.

Keywords

Combined cycle, Solar, Thermochemical Energy Storage, Limestone, CSP, Calcium-Looping, Solar Share, Dispatchability

1. Introduction

Increasing the energy storage capacity of the electric grid is a crucial issue to be solved in the short term [1]. Efficient, cost-effective and scalable energy storage systems stand as one of the main technological challenges for the massive deployment of renewable energies [2]. Among energy storage solutions, Thermal Energy Storage (TES) costs are one order of magnitude lower than Batteries Electrochemical Energy Storage [3,4]. This has aroused great interest in developing Concentrating Solar Power (CSP) plants coupled to TES systems capable of providing dispatchable power at a large scale. Commercial TES systems used in CSP plants are based on molten $NaNO_3/KNO_3$ salts [5]. However, molten salts-based systems suffer from several limitations that penalise the CSP plant performance, such as salts corrosiveness [6], limitation on the maximum temperature in the power cycle (~560ºC) to avoid salts degradation [7] and significant electric energy

consumption to keep salts at temperatures higher than ~220ºC to avoid salts solidification [8]. Alternatively, research in Thermochemical Energy Storage (TCES) systems is increasing in recent years. TCES systems integrated into CSP plants use solar energy to provoke an endothermic reaction. Under demand, the separately stored reaction products are brought together, and the opposite exothermic reaction takes place to release the stored energy. The cyclic calcination/carbonation of $CaCO_3$/CaO (Eq.1) presents excellent characteristics as an energy storage system for CSP plants [9,10]. Calcium Looping (CaL) TCES is characterised by a very high energy release temperature, high energy density and a low price of the raw materials (limestone or dolomite) [11,12].

$$CaCO_{3(s)} \rightleftarrows CaO_{(s)} + CO_2 \qquad \Delta H_r^0 = 178 \frac{kJ}{mol} \tag{1}$$

Currently, the most efficient CSP plants are based on superheated steam cycles with a maximum temperature of around 560ºC to allow integration with the molten salts system and state-of-the-art solar metallic receivers. Under these conditions, the current CSP technology presents power block efficiencies around 38% [13] with an annual solar-to-electricity conversion efficiency lower than 20% [5]. An interesting option is to integrate the CSP system with a Combined Cycle (CC). However, the current Integrated Solar Combined Cycles (ISCC) just cover a small share (typically lower than 15%) of the total thermal energy due to the impossibility of operating at high temperatures (>1000ºC required at gas turbine inlet) without solar radiation. Besides, there are no ISCC plants in current operation with energy storage, which makes them highly dependent on the use of fossil fuels [14]. Thus, the solar share, defined as the ratio between the solar thermal energy to the total energy, in large scale ISCC plants is only around 3-7% (i.e. Waad Al Shamal or Ain Beni Mathar plants), whilst at small scale, the maximum solar share reaches 13-14% (i.e. Hassi R'mel and Kuraymat plants) [13].

Many process schemes have been proposed to improve the CSP thermal integration in combined cycles [15]. Zhang et al. [16] developed a dynamic model to analyse the performance of two different ISCC schemes under selected days (~15% solar share). Even for extreme weather conditions, several operation strategies demonstrated a stable performance of the plan along the day. A dynamic model of the Hassi R'mel ISCC plant (~12% solar share) was developed in [17]. Results of the model predict in detail the actual results obtained in the operation of the plant. Montes et al. [18] considered a 50MWth hybridisation size in a 220MWe natural gas combined cycle (~23% solar share) with the preheating and boiling processes accomplished in the parabolic trough collectors. In [19], a CO2-based combined cycle, with supercritical and transcritical cycles as the topping and bottoming cycles, was proposed. On-design efficiencies of around 44% (excluding solar-side losses) were obtained for a turbine inlet temperature of 650ºC in the topping cycle (turbine inlet pressure of 160 bar). Ortiz et al. [20] proposed a CSP-CC integration through the CaL process by coupling an indirect power block integration with the carbonator where energy is released. Conlon [21] presented a dispatchable solar combined cycle from integrating a medium-temperature TES. A small scale SCC with sensible energy storage based on a fluidised particle solar receiver was proposed in [22]. The solar share was highly enhanced (theoretically up to 100%) since high-temperature energy storage was proposed, while solar-to-electric efficiency was found in the range of 20-25% for turbine inlet temperature up to 850ºC.

Direct integration of the CaL process in Solar Combined Cycles (SCC-TCES) has been recently proposed [14]. In a first conceptual approach, the proposed integration schemes reached overall efficiencies higher than 44% (excluding solar side losses). This novel concept allows operating a high-temperature gas turbine (as typical in CC) in a 24h pattern providing the necessary thermal power either from the solar receiver or the storage system. This is only possible from TCES able to work efficiently at high turning temperature (>900ºC) as is the case of the CaL process. In contrast, tower-based CSP plants that use molten salts for TES cannot be used to operate the combined solar cycle at night without significant fuel consumption. Despite the still low Technology Readiness Level (TRL) of TCES systems (TRL 4-5), the proposed SCC-TCES presents lower technical risks than previous studies of integrating these systems in solar plants. The main challenge in developing gas-solid TCES systems for solar applications is related to the solid particles receiver since the receiver has to provide energy for the exothermic reaction development within a certain residence time. Thus, the solar calciner represents higher cost uncertainty, and its performance highly conditions the overall efficiency [23]. As an improvement, the solar receiver in the SCC-TCES is a pressurized gas cavity, which has been tested at high temperatures at MW-scale [24] instead of a particle receiver.

The present work develops a deep analysis of the novel SCC-TCES plant. It extends the concept presented in [14], introducing advances and analysis for a better understanding of concept application. Two different integrations are considered and compared, one based on an air-open combined cycle and the other based on a CO_2 closed power cycle. Besides, the analyses are extended from a rated point to complete system modelling from representative days throughout the year, while the annual performance of the plant is estimated from a dedicated solar radiation clustering analysis. These advances in the model imply power plant sizing and optimisation for better integration with the solar field and receiver. Based on these new designs and conditions, characteristic off-design simulation and performance are developed. It allows the evaluation of the system performance under realistic operation conditions. In general, an attempt has been made in the present work to reduce the risk of the plant by using technology with a higher Technology Readiness Level than in [14]. Thus, a natural gas backup is incorporated into the cycle to guarantee the gas turbine operation during solar transients. It allows evaluating the hybridisation performance through the daily operation. Finally, new analyses have been carried out to analyse hybridisation scenarios based on the combustor chamber temperature, CO_2 emissions and optimum pressure ratio for a potential range of topping cycle turbine inlet temperature.

The results show an annual solar share in the combined cycles above 50%, which notably reduces CO_2 emissions of existing ISCC plants. Besides, the overall efficiency (excluding the solar side losses) expected is over 45%, which suggests the potential interest of further developing this process scheme.

2. A novel Calcium-Looping Solar Combined Cycle (SCC-TCES)

This work analyses the novel SCC-TCES plant, with the potential to notably improve the performance of CSP plants. The plant fully integrates CSP at high temperature (1200ºC) into a typical natural gas combined cycle from a high-temperature TCES system based on $CaCO_3$/CaO. It enhances solar contribution in combined cycles since the power block can operate at sunset without fossil fuel. Although the SCC-TCES concept has the

potential to operate with a 100% solar contribution, a natural gas backup is incorporated into the cycle to guarantee the gas turbine operation during solar transients. This serves to facilitate the potential scale-up of the proposed plant as operational risks of the novel system are reduced.

A conceptual scheme of the novel SCC-TCES plant is presented in Figure 1. The concept is based on a pressurised gas cavity receiver where an HTF is heated up to 1200ºC. Part of this solar energy (depending on the designed Solar Multiple -SM-) is stored in the TCES system while the rest drives the combined cycle. When solar radiation is not available, the TCES system provides the energy to operate the power block at the same conditions under solar operation. Two integration possibilities are modelled and compared in this work: i) a novel open-air combined cycle configuration (as illustrated in Figure 1) and ii) a CO_2 closed combined cycle as previously proposed in [14]. For the second case, Figure 1 is modified by including a new pipe between points 1-15 to close the HTF pathway and by considering an indirect combustor placed before the main turbine.

The SCC-TCES plant uses air (or CO_2 in the closed cycle) as Heat Transfer Fluid (HTF). If solar radiation is available, valve 'V2' is entirely closed, allowing the HTF passage to a high-temperature tubed cavity receiver, where it is heated up to temperatures around 1200ºC. Receiver efficiencies around 70-80% were reached at SOLUGAS facility for temperatures up to 800ºC [24], although lower efficiencies (50-55%) are expected in the present case due to radiation losses at such high temperature (1200ºC) [25].

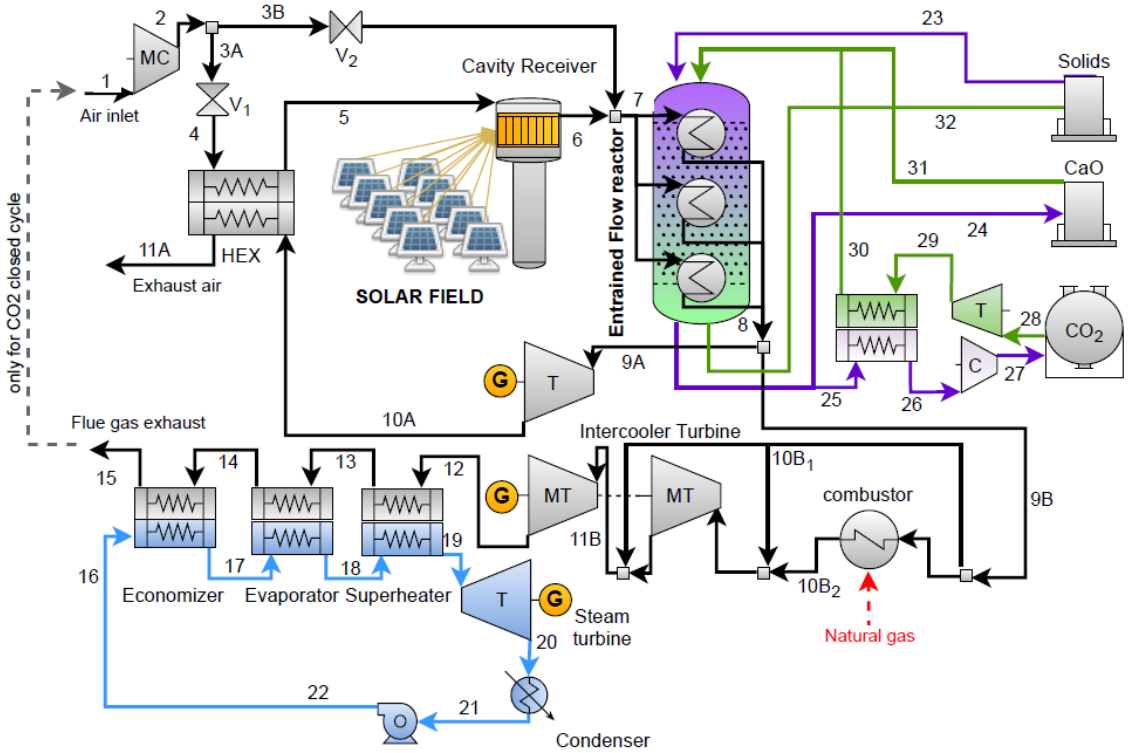

Figure 1: Conceptual scheme of the novel SCC-TCES plant. This scheme illustrates the air-combined cycle (the first case under analysis), while the CO_2 closed-cycle would include a pipe between lines 15→1 to close the cycle.

Later, the hot HTF stream transfers heat indirectly through a coiled heat exchanger connected to an Entrained Flow (EF) reactor [26], where energy storage starts from the calcination of $CaCO_3$ at 950ºC under pure CO_2 at atmospheric pressure, yielding CaO and CO_2. Under these conditions, the equilibrium temperature is ~ 896ºC [27], but calcination temperatures above 930ºC are necessary for a high development of decarbonation in short residence times [28]. As design criteria, if solar radiation is low (i.e. net thermal power provided is less than 40MWth), the HTF directly passes from the receiver to the Main Turbine (through a by-pass of the calciner). Under these conditions, there is no energy storage. EF reactors, which are well-known in the cracking industry, are emerging as a feasible technology to carry out the calcination of $CaCO_3$ as they allow using fine particles (dp<~50μm), which promotes calcination kinetics and mitigates the progressive loss of multicyclic CaO conversion [29,30]. Due to the high-volume flow of HTF, several parallel coils could be allocated along the reactor length. CaO is directly sent to a high-temperature silo by pneumatic conveying while the CO_2 must be cooled and compressed to minimise the storage tank volume [9]. Given the high temperatures, it is essential to efficiently use the sensible heat of the gases [31]. In the CO_2 storage process, the gas passes through a packed-bed tank filled with steel slag to charge a high-temperature energy storage system [14,32]. After that, the CO_2 pass in series through an intercooled compressor and a cooler to guarantee liquid storage conditions [9].

At the EF reactor exit (stream '8'), the HTF at around 1000ºC (after heat transfer for calcination) is split and expanded in two parallel turbines (T and MT in Figure 1) up to atmospheric pressure. A cooled stage turbine (blade-cooling) is considered in the main turbine (MT), using 5% of air extracted from the compressor to flow across the blades, cooling them by convection. At the auxiliary turbine (T) exit, the HTF is used to preheat the HTF entering the receiver in a regenerator (HEX). This increases the SM (and therefore, the plant's energy storage) (Ortiz et al., 2021) and reduces the thermal stresses in the receiver. A direct natural gas combustor is placed before the MT to heat the HTF up to 1150ºC, thus ensuring a constant temperature in the power cycle independently of solar radiation. At MT exit, the HTF (stream '12') passes through a Heat Recovery Steam Generator (HRSG). A single-pressure steam cycle with live steam conditions of 50 bar and 500ºC is proposed [13]. A higher efficiency (but implying also higher complexity) can be achieved by using a triple-pressure HRSG as proposed in [14].

Without solar radiation, the thermal energy starts to be transferred from the exothermic carbonation (Eq. 1) of the stored CaO under pure CO_2 in the EF reactor, from which the compressed HTF is heated in the absence of solar input (V2 open; V1 completely closed). While intercooling compression improves the performance under 'sun' mode, intercooling compression is not beneficial under 'night' operation mode since a better performance is obtained when HTF reaches the EF reactor at a higher temperature. Thus, turbine cooling should be able to be activated-deactivated depending on the operation strategy. This different behaviour under 'day' and 'night' modes involve a change in the optimum Pressure Ratio (PR) for each operation mode. As design criteria, a fixed PR that optimises at the same time the net power production under both operation modes has been selected. Carbonation is designed under pure CO_2 at 1000ºC and 8 bar to allow the same maximum temperature exit at EF reactor than in the sunshine hours (1000ºC) [14]. Under pressurised carbonation at 8 bar, the reaction equilibrium temperature is ~1070ºC, allowing carbonation at a fast rate [33]. Thus, the difference between the temperatures of calcination (950ºC) and carbonation (1000ºC) is small, which notably simplify the heat integration of the process, reducing the gas-solid heat exchangers and avoiding non-

mature solid-solid heat exchangers regarding previous process schemes [10]. Non-complete carbonation occurs in the CaL process. After several cycles, the CaO conversion decays to reach a certain residual value (Valverde et al., 2017), which depends on the calcination/carbonation conditions and the CaO precursor used [10]. A conservative value of Xr=0.15 for the residual CaO conversion after many cycles is assumed in the present work [34].

3. Modelling

A model of the proposed SCC-TCES concept has been developed using the commercial software Thermoflex® and Aspen Plus®. The Solar field has been sized using SolTrace [35] through a discrete Monte Carlo ray-tracing model, while the annual scaling up has been developed by a statistical model developed from Python.

As a first approach, to evaluate the plant performance under design conditions, two daily steady-state operation strategies are considered: 12h of constant solar input ('sun' mode) and 12h without solar input ('night' mode) [14]. Plant overall efficiency is determined as an average of the combined performance in both modes [34]. Later, a quasi-stationary hourly off-design model is simulated (see section 3.5) considering real solar patterns.

3.1. Solar field and receiver

A 360º heliostat solar field with three cavity receivers on top of a 200 m tower has been designed. The cavities are evenly spaced 120º, with one of them pointing straight at the geographic north. For simplicity and resources optimisation, only one subfield and the receiver have been implemented in the ray-tracing algorithm, which is computed three times with the appropriate solar azimuth offsets to account for the three cavities subfields. The layout of the heliostats has been derived from a biomimetic algorithm, which resembles a spiral (Figure 11 in the annexes section). Several parameters need to be adjusted for this layout to reduce the blocking effects among heliostats and the distance between adjacent heliostats, making a compromise for land use and solar efficiency. A spreadsheet has been used for the fine-tuning of parameters and coordinates generation.

Once the basic layout has been settled, one restriction will discard several heliostats to optimise the cost-benefit ratio: the aiming error of the heliostat (see in annexes section). From the CESA-I project at PSA, a value of 3 mrad in the reflected ray has been considered. This includes optical errors as well as tracking errors. The following algorithm is applied with these parameters: all the heliostats of a subfield whose reflected beam falls outside the receiver window are discarded. This imposes a penalty for heliostats that are farther and with a smaller view angle of the cavity, or which are too close to the tower and therefore the view angle again is small. The resulting subfield is shown in Figure 2.

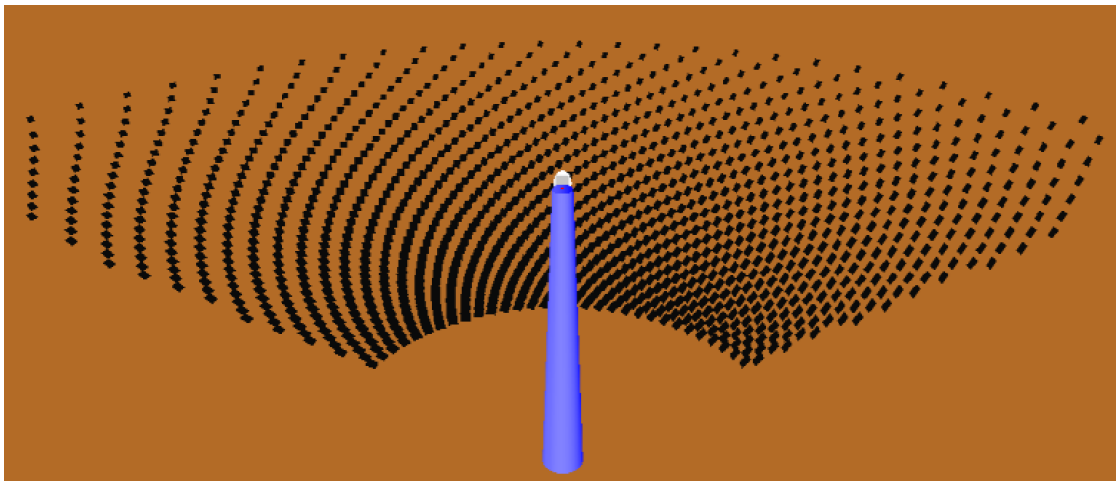

Figure 2: Resulting heliostats subfield (1/3 of the total)

A total of 1268 heliostats in each of the three subfields are simulated in the Soltrace ray-tracing software. Each heliostat is a 12 m x12 m mirror array, with a paraboloid of revolution shape, 1 km focal length, and specular reflectivity of 93%. Atmospheric attenuation losses have been simulated by adjusting the reflectivity of each heliostat as a function of the distance to the receiver due to the lack of such a model in Soltrace. This is an important factor in large tower plants because the atmospheric losses at 1,5 km are about 15% of the reflected power from the heliostat. For the ray-tracing, a script has been generated that calculates the solar vector at different hours of the day (using NOAA simplified model) and positions each heliostat in elevation and azimuth accordingly the reflected ray impacts at the centre of the receiver. Different strategies can be adopted here to avoid high flux gradients in the receiver without losing significant incident power.

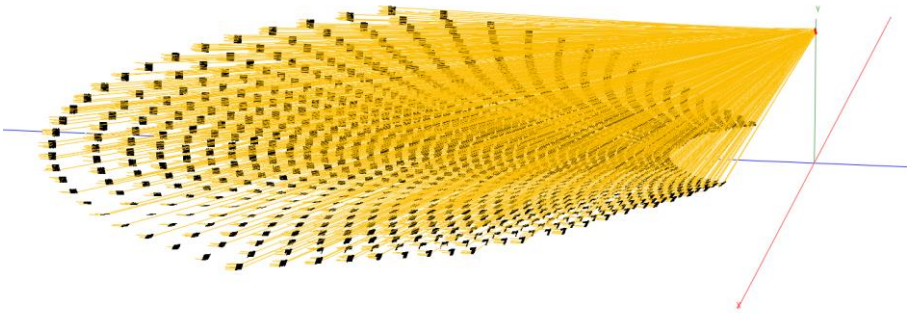

Figure 3: Ray-tracing simulation for the designed heliostats subfield

Once the solar field is set up for a given day of the year and time of day, up to 100 million rays are traced for that scene (Figure 3), and the solar flux at the receiver is obtained, from which the total incident power is calculated considering a 1000 W/m2 solar Direct Normal Irradiation (DNI). Later, the incident power is scaled with the actual DNI of a Typical Meteorological Year (TMY) data for the simulation (Seville, Spain), yielding the receiver's final incident power.

Importantly, flux density at the receiver (Figure 13 in Annex section) is in the same order of magnitude as existing gas receivers (e.g. SOLUGAS), and therefore technically feasible to build and operate. Due to the high temperature, SiC-based materials are

proposed for receiver pipes. SiC has a very high maximum allowable temperature beyond 1350ºC as well as very good mechanical properties up to this allowable temperature. The proposed pressure (less than 20 bar) is not a problem for the SiC-based pipes. A characteristic thickness that can handle up to 20 bar with the other more important thermo-mechanical loads also included would be 6.35 mm, for an external radius of 1.5875 cm (inner radius = 0.9525 cm). Regarding reliability of the concept, commercial systems as Siemens ETES (Electric Thermal Energy Storage) use air-based storage that can be coupled to CSP air-based receivers giving rise to a renewed interest in this type of technology in the context of hybrid CSP-PV plants [36]. On the other hand, there is also commercial technology available that use air-based receivers as those from the 247Solar company [37]. Therefore, the technology readiness level is high although some adaptation to the present context is required.

Each receiver is a flat panel of 12 m width and 8.4 m height, composed of a bundle of vertical pipes with a separation among them and a back reflective surface so that the pipes are irradiated more homogeneously from all angles. This assembly has not been modelled in this simulation, which is simplified as a continuous flat surface. Receiver losses should be modelled through a CFD, along with the incident solar flux and the ambient conditions (air temperature and speed, and sky temperature). The resulting calculation will account for convection and radiation losses, being the later great importance of the extremely high temperatures of 1200ºC achieved. Lacking this CFD simulation, a conservative value of 55% is supposed for thermal losses [6,25]. A quartz window is to be considered to limit the convection losses when performing more detailed simulations.

3.1.1. Annual plant performance through solar radiation data clustering

A data clustering technique is implemented to estimate the power plant's annual performance under different conditions. Data clustering aims to find groups in data [38] with similar features. Hence, the objective is to find a suitable number of clusters representing the entire data set, the centroid's position, and the data points that belong to each group.

Figure 4 shows solar data of a typical meteorological day for Seville, 37.4°N, 6.3°W, extracted from the "Photovoltaic Geographical information system" (PVGIS project) (European Commission, n.d.). The x-axis represents the number of sunshine hours, and the y-axis shows the daily solar irradiation (direct normal irradiation). The diagram displays the high difference between summer and winter seasons in Seville, where summer days have high solar irradiation and sunshine hours. In contrast, winter days have low solar irradiation and for just a few hours. In the data clustering process, the variables need to be scaled and converted to the same units. Then, both DNI and sunshine hours are scaled to dimensionless quantities in the interval [0,1]. As an approximation, it is considered each daily profile into two modes: a day mode with constant irradiance and a certain duration (sunshine hours); and a night mode with zero irradiance for the rest of the day [40] (see Figure 4b).

The silhouette analysis introduced by (Rousseeuw, 1987) will be used to select a suitable number of clusters. The annexe section details the procedure followed. The results confirm that 2, 3 or 4 clusters as representative days are suitable to estimate the performance of solar power technologies in Seville. Then, from a practical and perspective, four days, two of them representing winter and summer days, and two

representative clusters of the transition between winter and summer will be selected. Moreover, since the analysis of the performance for different scenarios is crucial to understanding the power plant's behaviour, optimum system configuration, and operation design, this clustering technique provides a reasonable annual estimation approach.

Once the number of clusters is defined, the next step is to optimise each centroid's location and the number of data points that belong to each cluster. Here, the k-means algorithm will be employed. The k-means algorithm, proposed by [41], starts by selecting a random position of one centroid for each cluster. Then it assigns every data point to the closest cluster by minimising the sum of the squared distance between each point and a centroid. Next, the algorithm iterates by re-locating the centroids in the centre of mass, i.e., the location where the weighted relative position of all points in the cluster sums up to zero. All data points are then assigned to the new centroids, and a new re-location of the centroids is performed. This algorithm is iterated until the location of the centroids does not move.

(a)

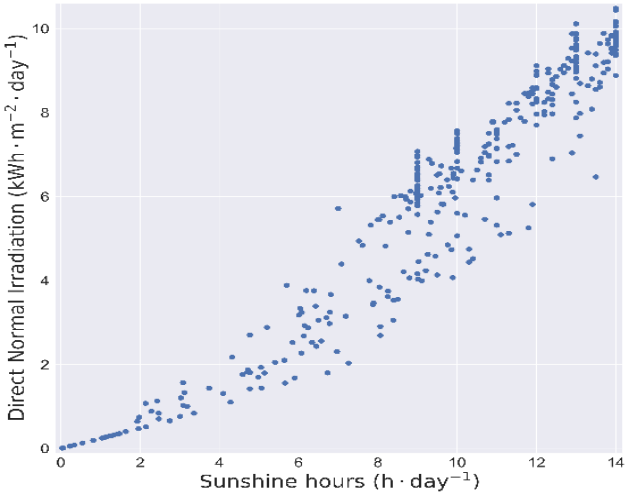

(b)

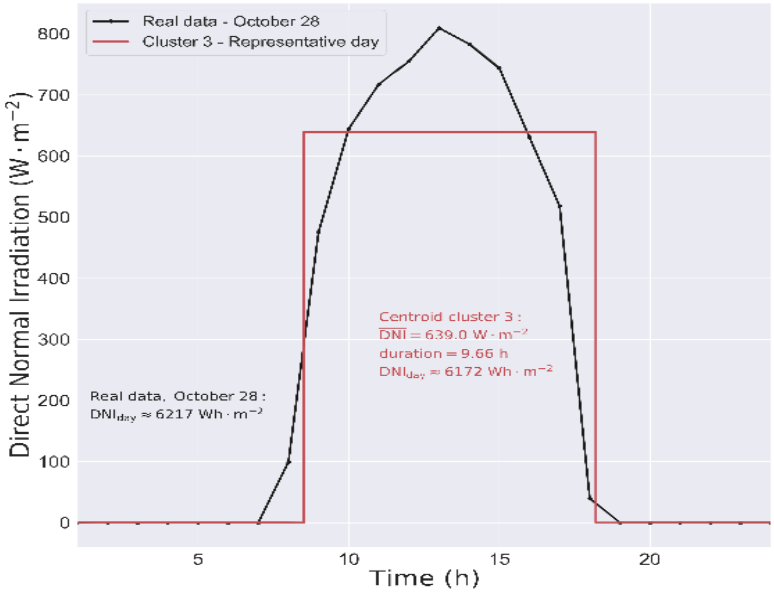

Figure 4: a) Typical meteorological year in Seville; b) Example of daily profiles using piecewise constant approximation.

Figure 5 and Table 1 show the data clustering results considering four representative days. The results illustrate four different scenarios representing practical weather conditions to evaluate the seasonal and annual performance of the solar power plant. As shown in the results, 35% of the data (129 days) is in the cluster with higher irradiation, represented by an average of 692.1 $W \cdot m^{-2}$. Then, 147 days are represented by a DNI = 639 $W \cdot m^{-2}$, 52 days by a DNI = 433.3 $W \cdot m^{-2}$, and finally, the group with the lowest solar irradiation is composed of 37 days (10%) represented by a day with DNI=319.9 $W \cdot m^{-2}$.

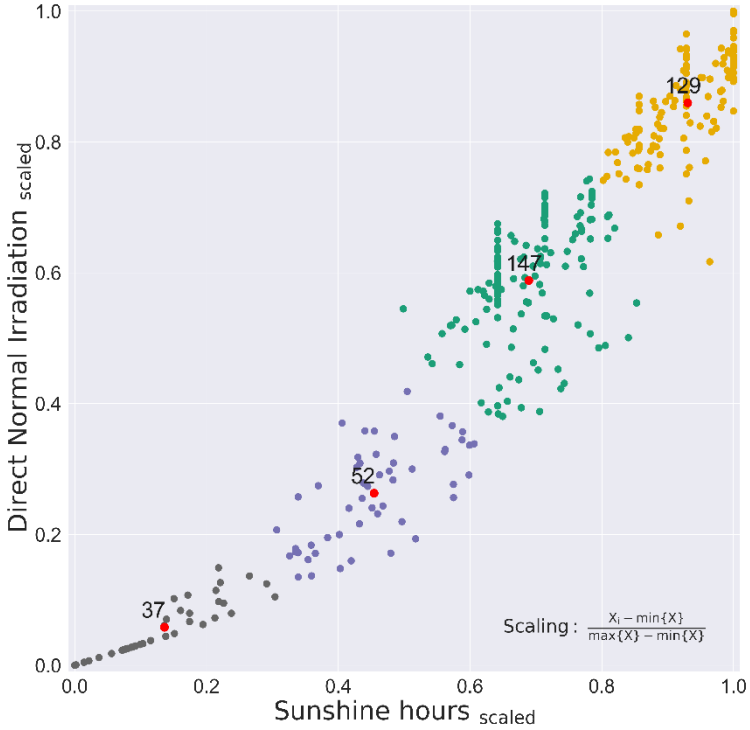

Figure 5: Data Clustering

The values of the DNI average ($W \cdot m^{-2}$) presented in Table 1 will be used in the next sections to simulate the performance of the power plant for each one of the four scenarios. The plant's annual performance estimation will then be assessed using the occurrence (%) of each scenario in a weighted average calculation.

Table 1: Data clustering results

Representative day	DNI ($Wh \cdot m^{-2} \cdot day^{-1}$)	Sunshine hours ($h \cdot day^{-1}$)	DNI average ($W \cdot m^{-2}$)	n (days)	Occurrence (%)
1	618.6	1.93	319.9	37	10.1
2	2763.3	6.38	433.3	52	14.2
3	6171.2	9.66	639.0	147	40.3
4	9017.7	13.03	692.1	129	35.4

The difference between the total annual solar irradiation using the complete data set throughout the year and the total amount according to the clustering process is less than 0.01 kWh/m^2. This minimal difference in the total annual irradiation, together with the use of daily profiles, supports the use of the data clustering process to simulate the solar power plant's operation, taking into account the daily and seasonal variability of the solar resource. The proposed simplification affects the average yearly value, but it does not

affect the hourly performance developed in section 4.1, which takes real hourly data to evaluate the performance (under off-design conditions) along the selected representative days. Thus, the off-design performance of the plant is evaluated hourly for each representative days, with a logical reduction of efficiency in the conditions furthest from the nominal situation (i.e. the first hours of the day). Once the average daily efficiency (affected by real solar radiation-dependent behaviour) has been obtained, the value is scaled annually depending on the occurrence of that characteristic day throughout the year.

3.2. TCES and power cycle

The main assumptions taken during the modelling are indicated in Table 2. The performance of the EF reactor is simplified by assuming a thermal efficiency of 95% for both calcination and carbonation stages. Under the H2020 SOCRATCES project (SOCRATCES project, 2018-2021), several works have developed EF reactor models to demonstrate the viability of this reactor under the proposed high-temperature conditions [43,44]. Results obtained in a recent work [26] show an HTF-to-solids overall heat transfer coefficient around 200 W/m^2K, which suggests that complete calcination could be reached less than 100s in a 50 m-length EF reactor under the same conditions that those presented in the present work.

Table 2: Main assumptions in the SCC-TCES model (see Figure 1)

Group	Parameter	Component	Value
Air-CO_2 turbomachinery	Isentropic efficiency	Turbines/compressors	92%
	Mechanical efficiency	Turbines/compressors	99%
	Intercooling/reheating	Main Compressor (MC)	2 stages (20ºC)
		CO_2 compressor (C)	4 stages (40ºC)
		CO_2 turbine (T)	3 stages (100ºC)
Pumps	Isentropic efficiency	All	85%
	Mechanical efficiency	All	99%
Steam turbine	Efficiency	-	90%
Generator	Efficiency	Gas turbine	99%
		Steam turbine	99%
Reactors	HTF pressure losses	Carbonator/calciner	2%
	conversion	calciner	100%
		carbonator	15%
	HTF thermal effectiveness	Carbonator/calciner	95%
Storage Vessels	Thermal losses	CO_2 storage, CFBs	0%
Heat exchangers	Pressure drop	HEX	1%
		Eco, Eva, Sup	2%
		Combustor	3.5%
	Heat losses	Combustor	2%
	Blowdown	Eva	1%
	Design Pinch	Eva	10ºC
	Minimum pinch	All steam cycle	3
	Thermal effectiveness	HEX	95%
		TES	95%
	Normalised heat losses	All	1%
Receiver	Thermal efficiency	-	55%
	Pressure drop	-	2%

All heat exchangers are assumed with a thermal efficiency of 95%. Thermal losses at the storage are dismissed in this work, although. With proper insulation, the hourly energy losses in the tanks could be around 0.18% per hour, even at such high temperatures [45,46]. Turbines are modelled to provide an adiabatic expansion with the same isentropic

efficiency in each stage. CO_2 properties are taken from REFPROP (NIST) database, whilst IFC-67 is used for steam properties formulation [14]. It is assumed in the model that turbines blades-cooling requires 5% of the total HTF flow. A condensing, single pressure steam turbine cycle is considered, with economiser, evaporator and superheater heat exchangers. A subcooling of 5ºC was defined at the economiser exit temperature.

3.3. Off-design modelling

This section describes the modelling considerations carried out to evaluate the plant performance under off-design conditions. As presented in section 3.1, the solar field performance is evaluated depending on the sun position through the model developed in SolTrace software. The steam turbine inlet temperature (500°C) and pressure (50 bar) are kept constant through an attemperator and a nozzle control, respectively [47]. Steam turbine efficiency calculation under off-design mode is calculated by assuming Thermoflex internal code [48]. The evaporator operation is controlled, keeping a minimum subcooling of 6ºC by introducing a recirculation stream.

Overall heat transfer coefficient (U) in all heat exchangers is scaling potentially with the mass flow with an exponent of 0.8 [47,49]. Design point overall heat exchange capability of the heat exchanger (UA) is kept constant. Pressure drops are calculated as a percentage of mass flows by introducing a flow resistance coefficient [47]. Thermal losses are considered as 1% of the heat transferred by the HTF.

A multistage centrifugal pump with fixed RPM and variable valve delta pressure is considered, whilst the isentropic efficiency of condenser pumps and fans is assumed constant [47]. For the HTF turbomachinery, mechanical efficiency is kept constant, while the isentropic efficiency degradation is automatically computed using the design software. For the intercooling compressor, the coolant flow is kept as 100% nominal. Turbines off-design efficiencies are calculated, assuming nozzle control. For simplicity, TCES and TES side turbomachinery and heat exchangers efficiencies are kept constants. EF and TES heat losses ratio are kept constant in off-design to 5% as in the design case.

4. Results and discussion

The proposed SCC-TCES plant was first evaluated at design conditions for each case: air-open and CO_2 closed combined cycles. Table 3 shows the main input for the simulations. In the design case, the total amount of energy stored during the 'day' mode is used under the 'night' mode. As design criteria, a constant mass flow of HTF through the power cycle at 'night' mode has been considered. In case that a certain power production pattern at 'night' would be required, this mass flow value would depend on the amount of energy to be produced. If the total energy released from the storage is not enough to heat the HTF mass flow at 'night' mode up to 1000ºC, the natural gas combustor will cover this difference. Pressure ratio has been chosen at the base case to provide efficient behaviour between considering jointly 'day' and 'night' operation modes. Later on, this PR value is optimised.

Table 3: Main parameters used for simulating the SCC-TCES plant at the design point

Group	Parameter	Value
Receiver	Net solar power	100 MWth
	Sunlight hours	12 h
Power block	TIT	1150ºC
	PR	12 (Air-open CC) 25 (CO_2-closed CC)
	Solar Multiple	1.35
	'Night' mode HTF mass flow	45 kg/s
	Live steam conditions	500ºC, 50 bar
	Average daily temperature	15ºC
	Relative humidity	60%
TCES	Average CaO conversion (X)	0.15
	Carbonator conditions	1000ºC, 8 bar
	Calcination conditions	950ºC, 1 bar
	CO_2 storage conditions	75 bar, 25ºC

The calculated energy balance is shown in Table 4. Most of the thermal power required for the power cycle is covered by the CSP at sunshine hours, reaching a solar share value as high as 94%. Without solar radiation, the previously stored energy provides around 50-55% of the total thermal requirements to cover a constant mass flow rate of 45 kg/s of HTF. This is a design criterion to keep almost constants power production at the main turbine; under other scenarios, a higher solar share would be provided from the storage if a lower amount of power production would be demanded and vice versa. Under this scenario, the overall daily solar share is above 72%, demonstrating the potential to boost the solar contribution in combined cycled, which currently presents solar shares below 15% [14]. A direct consequence of increasing the solar share is the reduction of the fossil fuel consumption compared with a Natural Gas Combined Cycle (NGCC) (or even current ISCC), which leads to a notable reduction in CO_2 emissions. Thus, CO_2 emissions would be around 110 kg/net MWhe, less than 1/3 of typical NGCC [50,51].

494 Table 4: SCC-TCES plant energy balance

	Parameter	Open-air CC		Closed-CO_2 CC	
		sun mode	night mode	sun mode	night mode
	Solar thermal power (MW_{th})	100	0	100	0
	Fuel consumption (LHV) (MW_{th})	6.20	21.08	8.92	19.86
Heat exchangers Thermal Power (MWth)	HXE	22.65	-	22.11	-
	CALCINER HE	22.83	-	22.83	-
	TES (net)	6.56	6.56	6.56	6.56
	CO_2 COOLER	2.25	-	2.25	-
	CO_2 HEATER	-	1.64	-	1.64
	CARBONATOR HE	-	21.41	-	21.41
	HP-COMP (intercooler)	1.81	-	1.81	-
	TURB1 (interheater)	-	1.12	-	1.12
	MC (intercooler)	17.98	-	23.68	-
	HRSG	14.16	19.6	26.54	26.95
	CONDENSER	8.96	12.4	16.80	17.06
Power production (MWe)	Main HTF turbine (MT)	22.85	31.44	27.06	27.83
	HTF turbine (T)	41.51	-	26.84	-
	Steam turbine	4.99	6.91	9.36	9.51
	CO2 storage turbine (HPT)	-	0.78	-	0.78
Power consumptions (MWe)	Main HTF Compressor (MC)	-26.78	-15.37	-21.04	-15.64
	CO_2 storage compressor (HPC)	-2.0	-	-2.0	-
	Steam cycle pumps	-0.04	-0.05	-0.07	-0.07
	Cooling pumps/fans	-0.23	-0.11	-0.35	-0.15
	Miscellaneous auxiliaries	-0.69	-0.23	-0.63	-0.21
	Generators losses	-0.71	-0.24	-0.65	-0.22
Summary	**$\dot{W}_{net}$ (MWe)**	**38.92**	**23.14**	**38.54**	**21.82**
	Solar share	**94.16%**	**50.39%**	**93.81%**	**55.3%**
	Average CO_2 emissions (kg/net MWhe)	**107.87**		**109.60**	
	Overall plant efficiency (excluding solar side losses)	**48.76%**		**46.87%**	

495

496 A key point on the design of dispatchable CSP systems is selecting the Solar Multiple (SM),
497 defined as the ratio of the receiver design thermal output to the power block design thermal
498 input. To enhance the energy storage capacity is proposed an HTF recirculation (stream 9a
499 in Figure 1). A higher inlet temperature reduces the ratio of solar thermal to calciner thermal
500 energy [14]. The amount of HTF recirculated is controlled through a split valve and the
501 receiver inlet HTF temperature. The SM value proposed in this work is relatively low, which
502 implies intra-week energy storage instead of seasonal energy storage as could be achieved
503 by larger thermochemical systems. Note that in the case of seasonal storage, the stored
504 materials should be kept at low temperature as proposed in [9]. However, higher SM values
505 involve larger solar side components, which would compromise the profitability of the plant
506 [52]. In addition, the higher the SM, the lower overall plant efficiency since the materials a
507 larger amount of CO_2 is compressed [34].

Expansion of the recirculated HTF provides an extra amount of electricity during sunshine hours. Markedly higher power consumption and production occur in the sun availability period because of the higher HTF flow for power production and charge the storage system. At night, without HTF recirculation due to energy stored requirements, a smaller mass flow of HTF must be compressed than at 'day' mode. Despite that the plant produces much more power under 'sun' mode operation, the power block efficiency is penalised because part of the power produced (2 MWe) is consumed to compress CO_2 up to the storage conditions.

As shown in Table 4, an overall plant efficiency (excluding solar side losses) above 48% is reached. Note that overall efficiency is calculated as an average of the 'sun' mode and 'night' modes [34]. This efficiency is higher than that shown in previous CSP-CaL integrations [10]. On the other hand, the efficiency reached is not an extraordinary result considering the power cycle used (combined cycle). However, the increase in efficiency with respect to existing solar plants and the increase in the solar share regarding typical ISCC is noteworthy. It should be underlined that there is a trade-off between the solar share and the ISCC efficiency because of the TIT. For a certain solar field size reaching a design temperature at the receiver, the higher the TIT, the higher plant efficiency and the lower the solar share since more natural gas must be burned to reach the TIT. This effect was also shown in previous works [53,54]. Figure 6 shows the daily solar share and the overall plant efficiency as a function of the TIT for the air-open case. The pressure ratio is selected, as indicated in Figure 7.

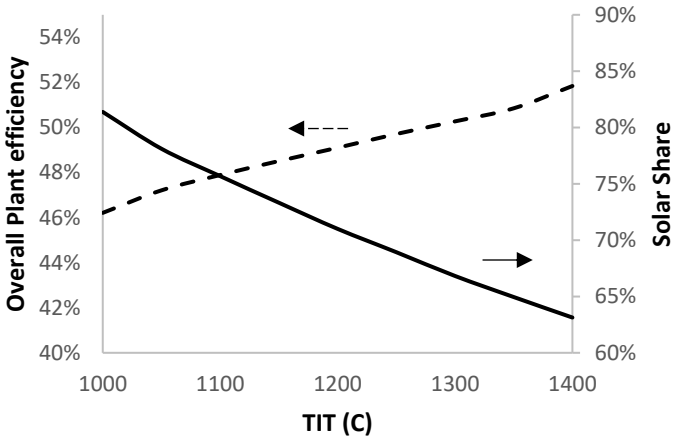

Figure 6: Overall plant efficiency and solar share as a function of the TIT. Note that PR is optimised for each TIT considered.

Overall efficiency values around 52% are reached if the TIT increases to 1400ºC (typical values in gas turbines), which would reduce the solar share of 20% points. Nevertheless, this solar share continues to be much higher than those obtained in typical ISCC plants (lower than 15%), because of integrating the TCES system. A similar SCC-TCES was proposed in [14] with a 100% solar share and a TIT of 1000ºC, reaching an overall plant efficiency of 45%.

Remarkably, as the TIT increases, the optimum PR also varies. To properly compare the scenarios in Figure 6, a sensitivity analysis on the PR for several values of TIT was carried out to maximize the power block efficiency (Figure 7a). The maximum values are approximate to integer values of PR. Note that the power block net electric efficiency considers the average value between 'day' and 'night' operation modes since the optimum

PR ratio is not the same for both modes. Optimum PR values for each TIT are illustrated in Figure 7b.

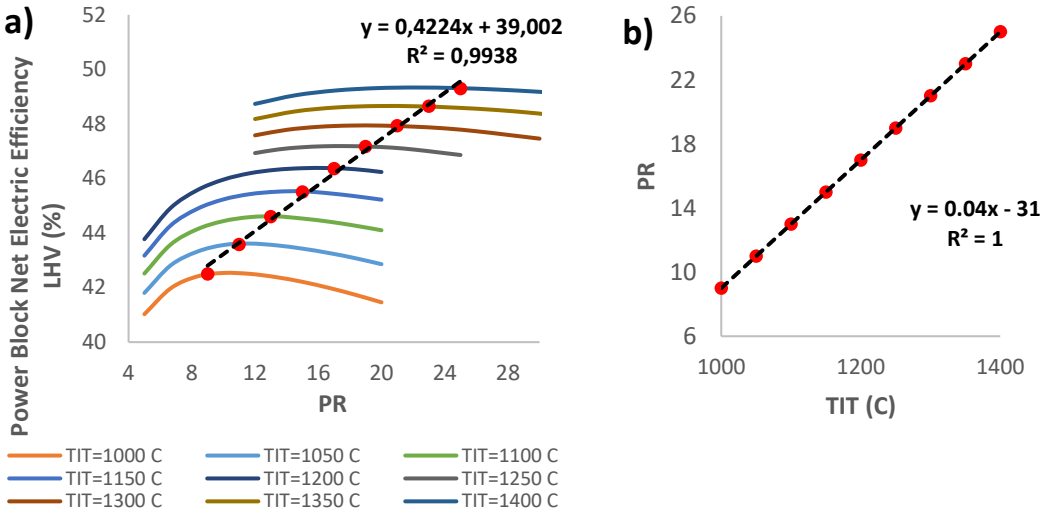

Figure 7: a) Power block net efficiency as a function of the PR for several values of TIT (air-open case); b) Optimum PR as a function of the TIT (air-open case).

By comparing both air-closed and CO_2-closed combined cycles, higher efficiency is reached in the former. The main difference is regarding the configuration of the HRSG, due to the CO_2 stream leaves the main gas turbine at a notably higher temperature (648.7ºC) than in the air case (549.8ºC). This involves a less efficient heat integration in small-sized steam turbines as in the present work (live steam conditions of 500ºC and 50 bar). The higher heat transferred into the HRSG involves almost duplicate the power produced in the steam turbine for the CO_2 closed-cycle but penalises the power production in the auxiliary turbine (T). Since the recirculated CO_2 (stream 15 in Figure 1) has a higher temperature than atmospheric (as in the air-open case), a lower amount of HFT to be recirculated is needed to achieve a certain SM than in the air case. Besides, a high compression work is required because of the higher HTF temperature at the compressor inlet. Despite these small differences, both cycles present a similar potential from the point of view of efficiency and CO_2 emissions. The higher density of the CO_2 allows a more compact solar receiver (also with lower thermal losses) and heat exchangers. On the other hand, closed combined cycles and specifically CO_2-based gas turbines are notably a less mature technology than open-air combined cycles.

4.1. Hourly behaviour

The SCC-TCES cycle (air-open case) has been simulated for representative days in Seville, taking real radiation patterns from a TMY. The main parameters used for the simulations are those shown in Table 3. Solar radiation and climatic data have been taken from PVGIS (European Commission, n.d.) whilst receiver thermal power and power block efficiency have been computed as described in section 3. As in the design case, it is assumed that all the energy stored in the sunshine hours is consumed at a constant rate during the rest of the day, and therefore there is a net balance equal to zero regarding the storage tanks. Figure 8 shows the disparity between these representative days' climatic conditions, which leads to extreme performances of the system. While the average solar share reaches 76% for a typical summer day (June 21), with milder solar radiation

conditions, the value is around 50%, which continues to be a very high value compared to existing ISCC plants [14]. For a better understanding of energy flows throughout the day, Figure 9 shows an hourly analysis of the amount of solar energy stored and the amount taken from the storage at sunset or the amount provided by the natural gas combustor as the backup system.

As showed in Table 4**,** a remarkably higher net power production is obtained at sunshine hours due to the contribution of the auxiliary turbine (T), with maximum values around 40 MWe, except for days with slight solar radiation (December 21), in which no energy would be stored. Therefore, the auxiliary turbine would be out of service. Note that this is an effect of the proposed configuration. Other operation strategies could be considered to adjust the net power production to a quasi-constant value throughout the day or to follow a certain dispatch pattern. In this sense, the TCES system as well as the natural gas combustor at the turbine inlet, give the system great flexibility.

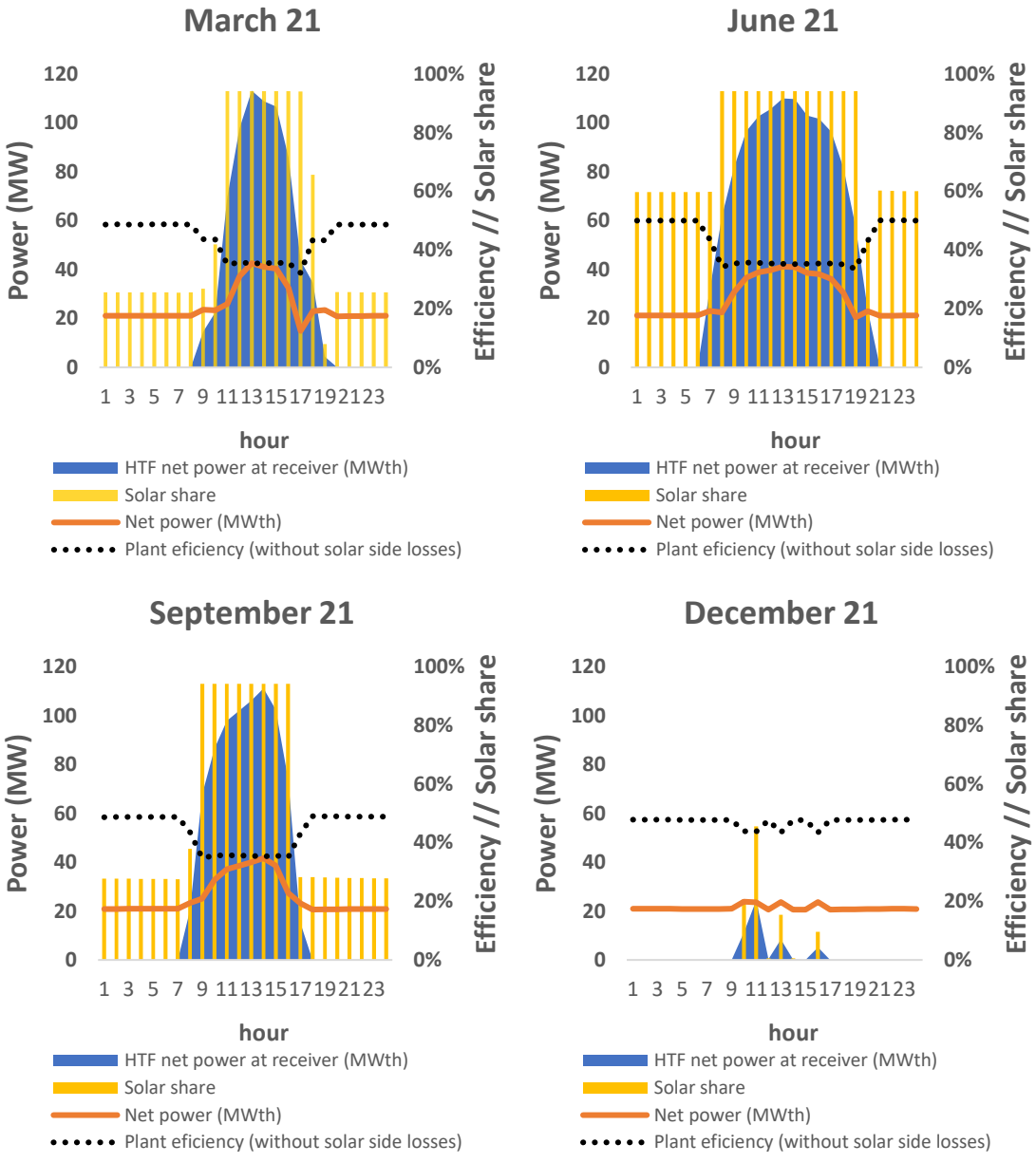

Figure 8: Hourly performance for selected days throughout the year.

The hourly plant efficiency follows a special pattern compared with commercial CSP plants since an important performance penalty occurs due to the power consumption of the turbomachines linked to the storage system. This is typical of solid-gas TCES systems [34]. Thus, hourly efficiency varies between 35-50%. Remarkably, the hourly efficiency is not computed as in Table 4, which was presented the overall plant efficiency. While the former (Figure 8) is calculated as the ratio between net electric power to the thermal power provided, even including the carbonator power, which is not a fuel or solar input since it comes from the storage, the overall (daily) plant efficiency computes the typical net electric power to the thermal (solar + fuel) input ratio. The influence of the off-design loss of efficiency is illustrated in Figure 15 (annexes section).

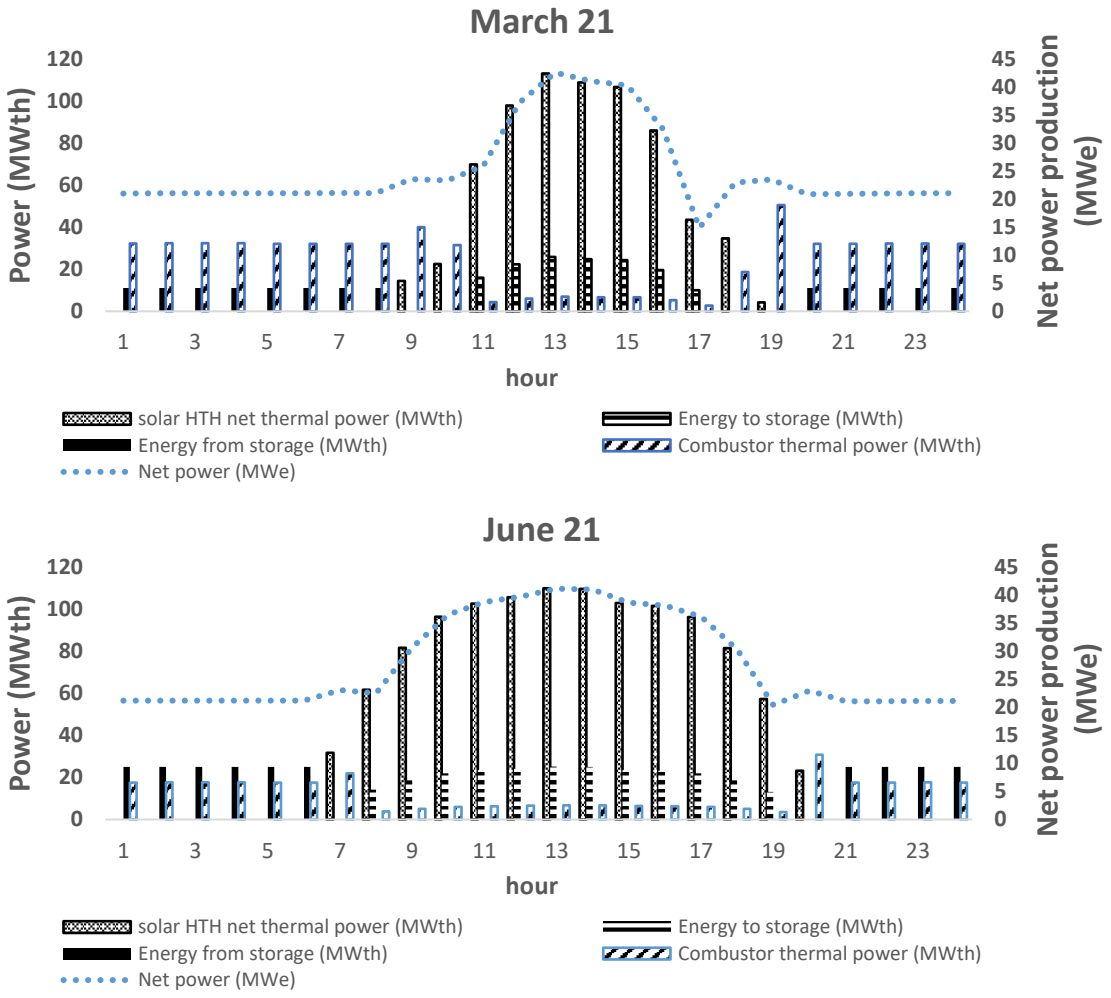

Figure 9: Hourly power production for selected days

As shown in Figure 9, on June 21, most of the power production throughout the night (60%) is obtained thanks to previously-stored solar energy, while the combustor contribution in sun hours is as low as 6%. On March 21, the constant power of 11MWth from the storage is produced from 8 pm to 8 am, representing a solar share of 26% in this interval.

Regarding storage tanks capacity, an analysis of the hourly variations of material flows makes it possible to estimate maximum and minimum amounts of material stored in the selected representative days (Figure 10). As may be seen, maximum and minimum

storage levels would occur in the highest solar radiation days. Considering June 21, in the first 6 hours of the day, CO_2 and CaO vessels are emptied as they are sent to the carbonator for power production while the solids ($CaO/CaCO_3$) storage is filled with solids from carbonation. After these hours, the solids tank has increased the material stored by 1535 tons while the amount of CaO and CO_2 in the storage tanks has been reduced in 1373 tons and 162 tons. Once solar energy harvesting begins, solids are sent to the calciner and CO_2 and CaO are produced and stored. Material stored in the solids tank is reduced up to -1045 tons compared to the beginning of the day. As a numerical example, if the day begins with 2000 tons of solids stored (CaO /CaCO3), along the day, the stored material will reach maximum (at 6 am) and minimum (at 17h) levels of 3535 tons and 955 tons respectively.

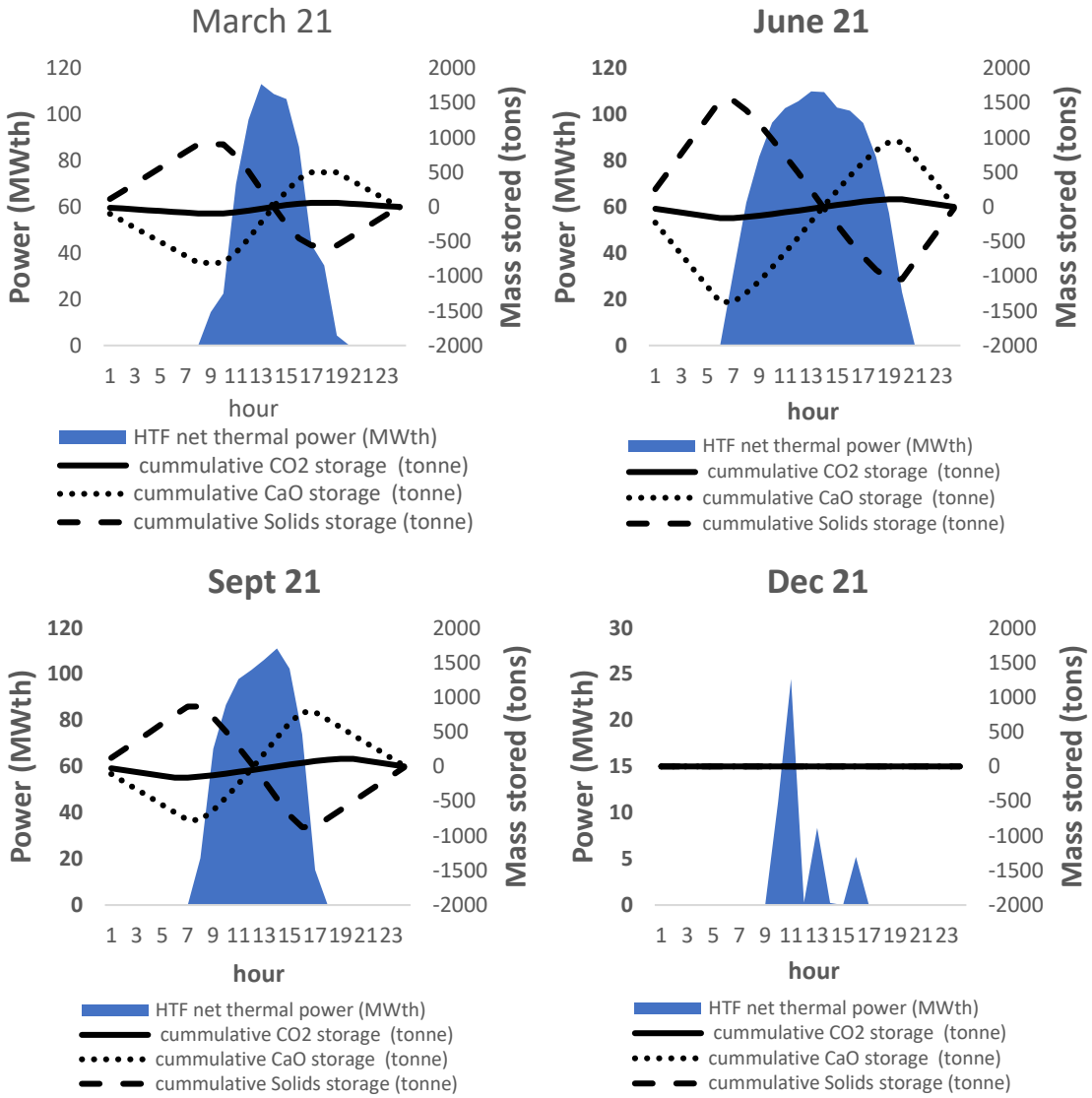

Figure 10: Analysis of the hourly flow of materials to and from the storage tanks. Note that the negative sign refers to the difference in the amount of material stored with respect to the beginning of the day.

The required amount of stored material depends fundamentally on the energy to be stored (which in turn is a function of the SM) as well as on the process conditions (mainly CO2 pressure, CO2 temperature and CaO conversion) [34]. The values represented in Figure

10 are in line with previous works found in the literature [47,55,56]. It is important to note that the optimal storage volume depends on the plant's strategies operation strategies, of high interest but which is beyond the scope of this work. Further optimisation of the operating strategy is required from a techno-economic perspective to reduce the energy storage cost ($/kWh) throughout the year.

4.2. Annual performance estimation

The annual performance of the plant has been estimated from the clustering process and taking real radiation and climatic data in Seville. The fourth representative days (used for clusters definition) are simulated from data collected in Table 1, assuming constant solar radiation (DNI) throughout the indicated solar hours and zero radiation the rest of the day. Note that constant DNI is assumed, but thermal power at the receiver varies depending on the solar position (azimuth, zenith). The cluster has been selected as follows: for the representative day 1, with slight solar hours, it is considered the solar position like December-21 (see Figure 8), while for the representative day 4 (Table 1), with up to 13 sunshine hours, it is considered the solar position as in June-21. Representative days 2 and 3 consider the solar position as March-21 and September-21, respectively. The analysis considers power production in the number of hours indicated in Table 1 around midday. The main results of the analysis for both air-open and CO_2 closed combined cycles are presented in Table 5.

Table 5: Annual performance estimation from solar radiation clustering

	Air-open CC					**CO_2-closed CC**				
Parameter	Day 1	Day 2	Day 3	Day 4	**Annual estimation**	Day 1	Day 2	Day 3	Day 4	**Annual estimation**
Receiver energy (GWh)	0.62	1.93	1.37	0.13	**488.89**	0.58	1.93	1.37	0.13	**485.36**
Solar net energy (GWh)	0.34	1.06	0.75	0.07	**268.89**	0.32	1.06	0.75	0.07	**266.95**
Combustor energy LHV (GWh)	0.72	0.29	0.47	0.99	**181.03**	0.71	0.30	0.48	0.97	**181.13**
Solar energy stored (GWh)	0.07	0.24	0.17	0.00	**60.92**	0.07	0.24	0.17	0.00	**60.51**
Electricity production (GWh)	0.89	1.15	1.04	0.90	**381.48**	0.83	1.08	0.98	0.84	**356.51**
Electricity consumption (GWh)	-0.40	-0.52	-0.47	-0.39	**-171.92**	-0.38	-0.45	-0.42	-0.38	**-153.82**
Electricity net (GWh)	0.49	0.63	0.57	0.50	**209.60**	0.45	0.62	0.56	0.45	**202.69**
Overall (daily) efficiency (%) (*)	46.29	46.39	46.70	47.35	**46.60%**	44.27	45.92	45.21	43.56	**45.16%**
Average emissions (kg/net MWh_e)	288.25	108.59	185.28	398.83	**192.35**	302.08	110.22	190.28	411.06	**198.09**
Average solar share (%)	32.28	74.57	56.08	5.77	**54.16**	30.27	74.62	55.62	5.28	**53.66**

(*) (without solar side losses). Computed as the ratio between net electric power to the total thermal input (solar + fuel).

The estimated annual performance results confirm the competitive results obtained for the SCC-TCES plant. Annual solar share is around 54% for both cases (air-open and CO_2 closed cycles), leading to a remarkable reduction in CO_2 emissions than existing NGCC plants. The annual net thermal-to-electric efficiency is above 45%. For an optimised solar receiver design, which minimises thermal losses by radiation and convection, the overall thermal-to-electric efficiency can be several %points higher than current CSP plants. Note that there is a relation between solar share and overall efficiency. The lower the solar share, the higher overall efficiency since the plant tends to appear more and more at an NGCC, without solar contribution. Remarkably, the higher solar share reached in the SCC-TCES is notably high than in previous works due to integrating a high-temperature energy storage system, which allows providing a relevant amount of solar power at sunset.

5. Conclusions

A novel Solar Combined Cycle – Thermochemical Energy Storage system (SCC-TCES) has been modelled and simulated, taking actual radiation data in Seville (Spain). Due to integrating an efficient TCES system, the combined cycle can operate at night from solar energy previously-stored at high temperature. This is only possible from TCES that work efficiently at high turning temperature (>900ºC), as is the calcium-looping ($CaCO_3$/CaO) process. Thus, considering actual solar data, the annual solar share is highly enhanced compared to current integrated solar combined cycle power plants (above 50% instead of 4-15%). This reduces the typical CO_2 emissions of the natural gas combined cycle by more than half, reaching values of around 100-200 kg/net MWhe, which would be equivalent to a CO_2 capture of around 75-85% in coal-fired power plants.

Four clusters (representative days) were selected from the solar radiation clustering analysis to evaluate the annual performance. Daily and annual average results confirm a high thermal-to-electric efficiency (45-50%) for both air-open and CO_2- closed cycles. As TIT increases, the overall plant efficiency is enhanced while the solar share is penalized. For a TIT of 1400ºC, overall plant efficiency would reach 52% with a solar share above 60%. Slightly higher efficiency is reached by the air-open configuration, although the CO_2-closed cycle offers the possibility of a more compact and efficient solar receiver design but also with a notably less mature level of technology. This offers the potential to boost the plant capacity regarding the state-of-the-art of CSP plants due to integrating efficient TCES and high-efficiency power blocks (combined cycle).

Remarkably, an optimum receiver design that minimizes solar radiation losses is crucial for the viability of this concept. This requires a more detailed study than presented in this work, followed by a suitable prototyping and scaling process. Efficiencies below 50% could compromise the technical viability of the plant. Besides, regarding previous CSP-TCES integrations, this novel concept here presented minimizes the gas-solids heat exchangers, and it avoids solid-solid heat exchangers, which are not yet commercial, and therefore gaining in plant reliability. Finally, the integration of a natural gas combustor at the inlet of the gas turbine provides the system with greater flexibility and reduces the risk of a shutdown of the plant in the event of a failure of the TCES system.

All these relevant features justify the potential interest in the SCC-TCES plant.

ACKNOWLEDGEMENTS

The research leading to these results has received funding from the European Union's Horizon 2020 research and innovation programme under grant agreement No 727348, project SOCRATCES, and by the Spanish Government Agency Ministerio de Economía y Competitividad (MINECO-FEDER funds) under contracts CTQ2017- 83602-C2 (-1-R and -2-R).

ABBREVIATIONS

CaL	Calcium-Looping
CC	Combined Cycle
CFB	Circulated Fluidised Bed
CSP	Concentrating Solar Power
DNI	Direct Normal Irradiation
DSG	Direct Steam Generation
EF	Entrained Flow
HTF	Heat Transfer Fluid
HRSG	Heat Recovery Steam Generator
ISCC	Integrated Solar Combined Cycles
PR	Pressure Ratio
SCC	Solar Combined Cycle
SM	Solar Multiple
TCES	Thermochemical Energy Storage
TES	Thermal Energy Storage
TIT	Turbine Inlet Temperature
TMY	Typical Meteorological Year

ANNEXES

A1. Solar field modelling

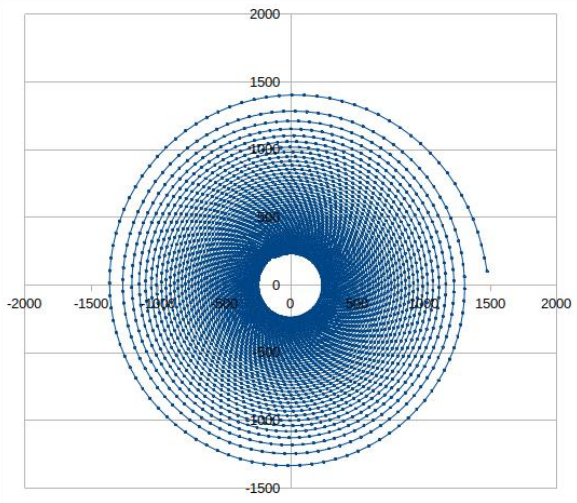

Figure 11: Heliostats field pre-design (distances to the origin in meters).

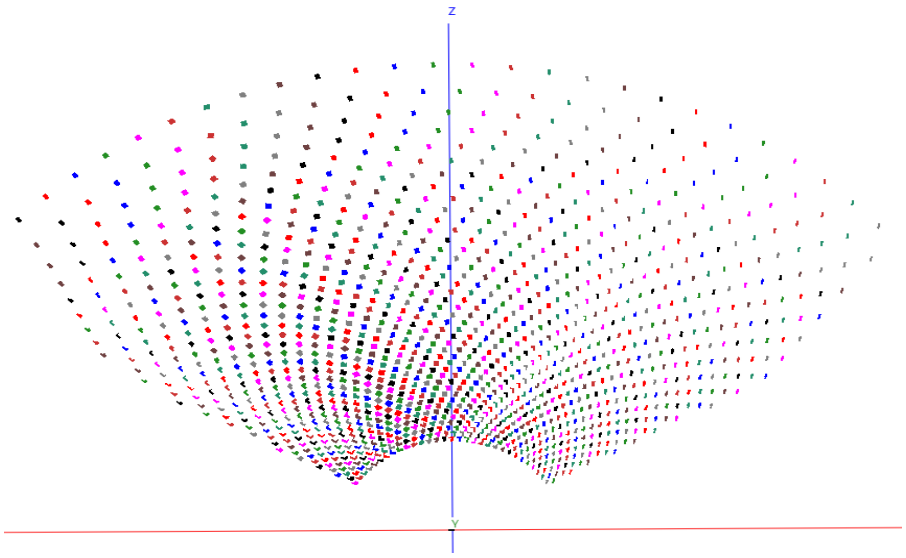

Figure 12: Heliostats field improved design.

A2. Solar flux at the receiver (W/m2)

This figure represents the geometry of the solar receiver panel, being the x-axis the horizontal direction and the y-axis in the vertical direction. The scale is in meters, being the origin (0,0) in the centre of the panel (that is why there are negative values in the x and y axes). Therefore the colour indicates the intensity of the solar flux in each position of the receiver panel. This simulation's location is Sevilla (Spain), already mentioned in the text, and the apparent solar position is 45º elevation and 135º azimuth, which corresponds to March 25th, at 11:30 local time.

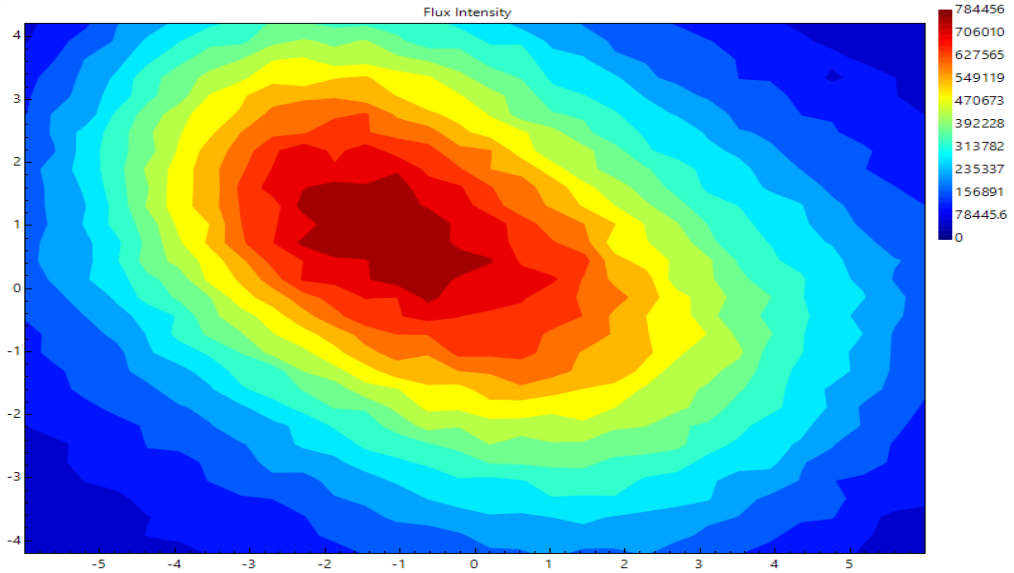

Figure 13: Solar flux at the receiver (W/m^2).

A3. Clustering

The silhouette analysis measures the distance between each data point with the neighbouring clusters and computes a numerical value in the range [-1, 1]. A value close to 1 denotes that the point is distant from the neighbouring clusters; therefore, the observations are well clustered. A value close to 0 indicates that the point lies at the boundary between two clusters. Finally, a negative value shows that the data point is probably assigned to the wrong cluster.

Figure 14 displays the result of the silhouette analysis from 2 to 30 clusters.

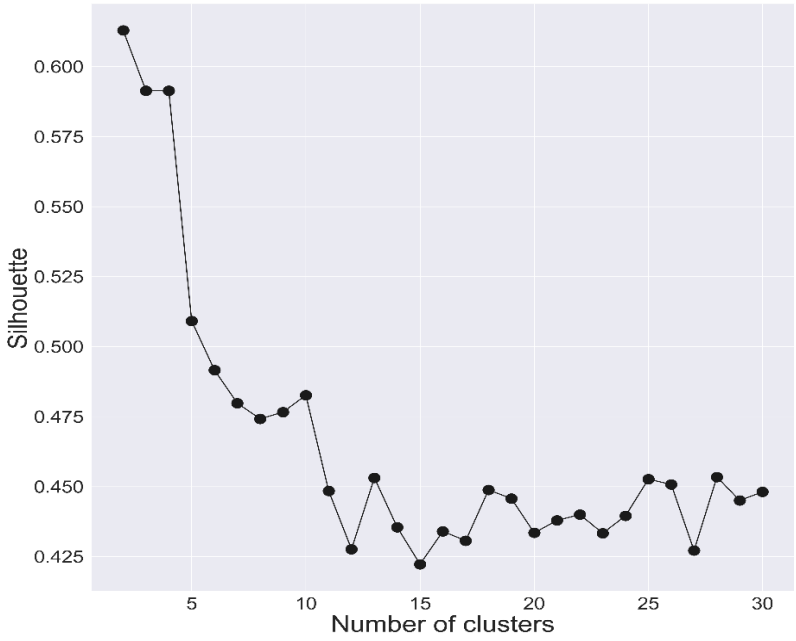

Figure 14: Silhouette Analysis

A4. Stream data

Table 6: Stream data for the air-open CC at design conditions (see Figure 1 and Table 4)

	'sun' mode				'night' mode		
stream id	materials	P (bar)	T(ºC)	m (kg/s)	P (bar)	T(ºC)	m (kg/s)
1	Air	1.01	15	100.3	1.01	15	45
2	Air	12.78	108.5	100.3	12.4	344.7	45
3A	Air	12.78	108.5	100.3	12.4	344.7	0
3B	Air	12.78	108.5	0	12.4	344.7	45
4	Air	12.78	108.5	100.3	-	-	-
5	Air	12.65	327.0	100.3	-	-	-
6	Air	12.4	1200.0	100.3	-	-	-
7	Air	12.4	1200.0	100.3	12.4	344.7	45
8	Air	12.16	1000	100.3	12.16	772	45
9A	Air	12.16	1000	67.31	-	-	-
9B	Air	12.16	1000	32.99	12.16	772	45
10A	Air	1.01	452.2	67.31	-	-	-
10B1	Air	11.75	1000	0.82	11.75	772	1.12
10B2	Air	11.75	1146.2	32.3	11.75	1140.9	44.33
11A	Air	1.00	126.2	67.31	-	-	-
11B	Air	5.34	923.1	33.13	5.34	915.8	45.46
12	Air	1.02	549.8	33.13	1.02	548	45.46
13	Air	1.02	474.9	33.13	1.02	473.6	45.46
14	Air	1.01	275.2	33.13	1.01	275,2	45.46
15	Air	1.01	150.5	33.13	1.01	151.2	45.46
16	Water	52.02	33.57	4.29	52.02	33.57	5.94
17	Water	51	260.2	4.29	51	260.2	5.94
18	Steam	51	265.2	4.25	51	265.2	5.88
19	Steam	50	500	4.25	50	500	5.88
20	Steam	0.05	32.88	4.25	0.05	32.88	5.88
21	Water	0.05	32.9	4.25	0.05	32.9	5.88
22	Water	52.02	33.57	4.29	52.02	33.57	5.94
23	CaCO3/CaO	1.00	1000	64.61	-	-	
24	CaO	1.00	950	57.81	-	-	-
25	CO_2	1.00	950	6.81	-	-	-
26	CO_2	1.00	110	6.81	-	-	-
27	CO_2	75.00	25	6.81	-	-	-
28	CO_2	-	-	-	75.00	25	6.81
29	CO_2	-	-	-	8.05	100	6.81
30	CO_2	-	-	-	8.04	937.7	6.81
31	CaO	-	-	-	1.00	925	57.81
32	CaCO3/CaO	-	-	-	1.00	1000	64.61

A5. Design and off-design performance comparison for a selected day

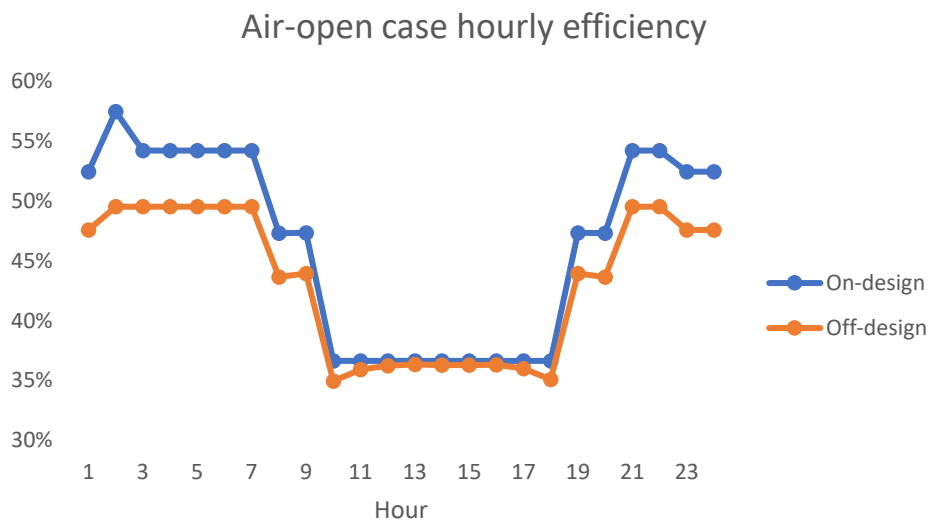

Figure 15: Design and Off- design performance comparison

REFERENCES

[1] U.S. Department of Energy. Energy Storage Grand Challenge 2020.

[2] Panwar NL, Kaushik SC, Kothari S. Role of renewable energy sources in environmental protection: A review. Renew Sustain Energy Rev 2011;15:1513–24. https://doi.org/10.1016/j.rser.2010.11.037.

[3] Cole W, Frazier AW. Cost Projections for Utility-Scale Battery Storage. 2019.

[4] Rahman MM, Oni AO, Gemechu E, Kumar A. Assessment of energy storage technologies: A review. Energy Convers Manag 2020;223:113295. https://doi.org/10.1016/j.enconman.2020.113295.

[5] Islam MT, Huda N, Abdullah AB, Saidur R. A comprehensive review of state-of-the-art concentrating solar power (CSP) technologies: Current status and research trends. Renew Sustain Energy Rev 2018;91:987–1018. https://doi.org/10.1016/j.rser.2018.04.097.

[6] Ho CK. A review of high-temperature particle receivers for concentrating solar power. Appl Therm Eng 2016;109:958–69. https://doi.org/10.1016/j.applthermaleng.2016.04.103.

[7] Kearney D, Kelly B, Herrmann U, Cable R, Pacheco J, Mahoney R, et al. Engineering aspects of a molten salt heat transfer fluid in a trough solar field. Energy 2004;29:861–70. https://doi.org/10.1016/S0360-5442(03)00191-9.

[8] Vignarooban K, Xu X, Arvay A, Hsu K, Kannan AM. Heat transfer fluids for concentrating solar power systems - A review. Appl Energy 2015;146:383–96. https://doi.org/10.1016/j.apenergy.2015.01.125.

[9] Chacartegui R, Alovisio A, Ortiz C, Valverde JMM, Verda V, Becerra JAA. Thermochemical energy storage of concentrated solar power by integration of the calcium looping process and a CO2 power cycle. Appl Energy 2016;173:589–605. https://doi.org/10.1016/j.apenergy.2016.04.053.

[10] Ortiz C, Valverde JM, Chacartegui R, Perez-Maqueda LA, Giménez P. The

Calcium-Looping (CaCO3/CaO) process for thermochemical energy storage in Concentrating Solar Power plants. Renew Sustain Energy Rev 2019;113:109252. https://doi.org/10.1016/j.rser.2019.109252.

[11] Tesio U, Guelpa E, Verda V. Integration of thermochemical energy storage in concentrated solar power. Part 1: Energy and economic analysis/optimization. Energy Convers Manag X 2020;6:100039. https://doi.org/10.1016/j.ecmx.2020.100039.

[12] Tesio U, Guelpa E, Verda V. Integration of ThermoChemical Energy Storage in Concentrated Solar Power. Part 2: comprehensive optimization of supercritical CO2 power block. Energy Convers Manag X 2020;6:100038. https://doi.org/10.1016/j.ecmx.2020.100038.

[13] National Renewable Energy Laboratory (NREL). Concentrating Solar Power Projects 2017. https://www.nrel.gov/csp/solarpaces/index.cfm (accessed July 1, 2018).

[14] Ortiz C, Chacartegui R, Valverde JM, Carro A, Tejada C, Valverde J. Increasing the solar share in combined cycles through thermochemical energy storage. Energy Convers Manag 2021;229:113730. https://doi.org/10.1016/j.enconman.2020.113730.

[15] Khandelwal N, Sharma M, Singh O, Shukla AK. Recent Developments in Integrated Solar Combined Cycle Power Plants. J Therm Sci 2020;29:298–322. https://doi.org/10.1007/s11630-020-1278-2.

[16] Zhang N, Duan L, Huang C, Hou H, Yu G, Ding Z, et al. Operation strategy and dynamic performance study of integrated solar combined-cycle system. Energy Convers Manag 2021;228:113716. https://doi.org/10.1016/j.enconman.2020.113716.

[17] Abdelha N, Halil İ, El N, Bachari I. An innovative dynamic model for an integrated solar combined cycle power plant under o ff -design conditions 2020;220. https://doi.org/10.1016/j.enconman.2020.113066.

[18] Montes MJ, Rovira A, Muñoz M, Martínez-val JM. Performance analysis of an Integrated Solar Combined Cycle using Direct Steam Generation in parabolic trough collectors. Appl Energy 2011;88:3228–38. https://doi.org/10.1016/j.apenergy.2011.03.038.

[19] Khatoon S, Kim M. Performance analysis of carbon dioxide based combined power cycle for concentrating solar power. Energy Convers Manag 2020;205:112416. https://doi.org/10.1016/j.enconman.2019.112416.

[20] Ortiz C, Chacartegui R, Valverde JMM, Alovisio A, Becerra JAA. Power cycles integration in concentrated solar power plants with energy storage based on calcium looping. Energy Convers Manag 2017;149:815–29. https://doi.org/10.1016/j.enconman.2017.03.029.

[21] Conlon WM. Dispatchable solar combined cycle. ASME 2017 11th Int Conf Energy Sustain ES 2017, Collocated with ASME 2017 Power Conf Jt with ICOPE 2017, ASME 2017 15th Int Conf Fuel Cell Sci Eng Technol ASME 201 2017:1–7. https://doi.org/10.1115/ES2017-3578.

[22] Behar O, Grange B, Flamant G. Design and performance of a modular combined cycle solar power plant using the fluidized particle solar receiver technology. Energy Convers Manag 2020;220:113108. https://doi.org/10.1016/j.enconman.2020.113108.

[23] Bravo R, Ortiz C, Chacartegui R, Friedrich D. Hybrid solar power plant with thermochemical energy storage: A multi-objective operational optimisation. Energy Convers Manag 2020;205:112421.

https://doi.org/10.1016/j.enconman.2019.112421.
[24] Korzynietz R, Brioso JA, Del Río A, Quero M, Gallas M, Uhlig R, et al. Solugas - Comprehensive analysis of the solar hybrid Brayton plant. Sol Energy 2016;135:578–89. https://doi.org/10.1016/j.solener.2016.06.020.
[25] Sedighi M, Padilla RV, Taylor RA, Lake M, Izadgoshasb I, Rose A. High-temperature, point-focus, pressurised gas-phase solar receivers: A comprehensive review. Energy Convers Manag 2019;185:678–717. https://doi.org/10.1016/j.enconman.2019.02.020.
[26] Ortiz C, Valverde J, Tejada C, Carro A, Chacartegui R. Solar-Driven Indirect Calcination for Thermochemical Energy Storage (UNPUBLISHED WORK). SolarPACES Int. Conf., 2020.
[27] Barin I. Thermochemical data of pure substances VCH, Weinheim (1989) 1989.
[28] Valverde JM, Sanchez-Jimenez PE, Perez-Maqueda L. Calcium-looping for post-combustion CO2 capture. On the adverse effect of sorbent regeneration under CO2. Appl Energy 2014;126:161–71. https://doi.org/10.1016/j.apenergy.2014.03.081.
[29] Benitez-Guerrero M, Sarrion B, Perejon A, Sanchez-Jimenez PE, Perez-Maqueda LA, Manuel Valverde J. Large-scale high-temperature solar energy storage using natural minerals. Sol Energy Mater Sol Cells 2017;168:14–21. https://doi.org/10.1016/j.solmat.2017.04.013.
[30] Durán-Martín JD, Sánchez Jimenez PE, Valverde JM, Perejón A, Arcenegui-Troya J, García Triñanes P, et al. Role of particle size on the multicycle calcium looping activity of limestone for thermochemical energy storage. J Adv Res 2020;22:67–76. https://doi.org/10.1016/j.jare.2019.10.008.
[31] Chen X, Zhang D, Wang Y, Ling X, Jin X. The role of sensible heat in a concentrated solar power plant with thermochemical energy storage. Energy Convers Manag 2019;190:42–53. https://doi.org/10.1016/j.enconman.2019.04.007.
[32] Ortega-Fernández I, Calvet N, Gil A, Rodríguez-Aseguinolaza J, Faik A, D'Aguanno B. Thermophysical characterization of a by-product from the steel industry to be used as a sustainable and low-cost thermal energy storage material. Energy 2015;89:601–9. https://doi.org/10.1016/j.energy.2015.05.153.
[33] Ortiz C, Valverde JM, Chacartegui R, Perez-Maqueda LA. Carbonation of Limestone Derived CaO for Thermochemical Energy Storage: From Kinetics to Process Integration in Concentrating Solar Plants. ACS Sustain Chem Eng 2018;6:6404–17. https://doi.org/10.1021/acssuschemeng.8b00199.
[34] Ortiz C, Romano MC, Valverde JM, Binotti M, Chacartegui R. Process integration of Calcium-Looping thermochemical energy storage system in concentrating solar power plants. Energy 2018;155:535–51. https://doi.org/10.1016/j.energy.2018.04.180.
[35] Ho CK. Software and Codes for Analysis of Concentrating Solar Power Technologies. 2008.
[36] International Renewable Energy Agency. Innovation Outlook: Thermal Energy Storage. 2020.
[37] 247solar company. Clean power solutions n.d. https://www.247solar.com/ (accessed April 1, 2021).
[38] Kaufman L, Rousseeuw PJ. Finding Groups in Data: An Introduction to Cluster Analysis. volume 180. NJ, USA: JohnWiley & Sons, Inc.; 2005.
[39] European Comission. Photovoltaic geographical information system (PVGIS) n.d.
[40] Peng X, Yao M, Root TW, Maravelias CT. Design and Analysis of Concentrating

Solar Power Plants with Fixed-bed Reactors for Thermochemical Energy Storage. Appl Energy 2020;262:114543. https://doi.org/10.1016/j.apenergy.2020.114543.
[41] MacQueen J. Some methods for classification and analysis of multivariate observations. Proc. Fifth Berkeley Symp. Math. Stat. Probab. Vol. 1 Stat., Berkeley, Calif.: University of California Press; 1967, p. 281–97.
[42] SOCRATCES project Consortium. Socratces Project 2018. https://socratces.eu/.
[43] Lisbona P, Bailera M, Hills T, Sceats M, Díez LI, Romeo LM. Energy consumption minimization for a solar lime calciner operating in a concentrated solar power plant for thermal energy storage. Renew Energy 2020;156:1019–27. https://doi.org/10.1016/j.renene.2020.04.129.
[44] Bailera M, Lisbona P, Romeo LM, Díez LI. Calcium looping as chemical energy storage in concentrated solar power plants: Carbonator modelling and configuration assessment. Appl Therm Eng 2020:115186. https://doi.org/10.1016/j.applthermaleng.2020.115186.
[45] Miller JE, Ambrosini A, Babiniec SM, Coker EN, Ho CK, Al-Ansary H, et al. High performance reduction/oxidation metal oxides for thermochemical energy storage (PROMOTES). ASME 2016 10th Int Conf Energy Sustain ES 2016, Collocated with ASME 2016 Power Conf ASME 2016 14th Int Conf Fuel Cell Sci Eng Technol 2016;1:1–8. https://doi.org/10.1115/ES2016-59660.
[46] Peng X, Yao M, Root TW, Maravelias CT. Design and analysis of concentrating solar power plants with fixed-bed reactors for thermochemical energy storage. Appl Energy 2020;262:114543. https://doi.org/10.1016/j.apenergy.2020.114543.
[47] Ortiz, Binotti M, Romano MC, Valverde JM, Chacartegui R. Off-design model of concentrating solar power plant with thermochemical energy storage based on calcium-looping. vol. 210006, 2019, p. 210006. https://doi.org/10.1063/1.5117755.
[48] Thermoflow Inc. Thermoflex, Fully-flexible design and simulation of conventional steam plants, combined cycles, and other thermal power systems n.d.
[49] Patnode AM. Simulation and performance evaluation of parabolic trough solar power plants. Univ Wisconsin-Madison 2006;Master:5–271.
[50] NETL. Cost and Performance Baseline for Fossil Energy Plants Volume 1a: Bituminous Coal (PC) and Natural Gas to Electricity, Revision 3, vol. DOE/NETL-2015/1723 2015;1.
[51] CAESAR project. European best practice guidelines for assessment of CO2 capture technologies. 2011.
[52] Tapachès E, Salas D, Perier-Muzet M, Mauran S, Aussel D, Mazet N. The value of thermochemical storage for concentrated solar power plants: Economic and technical conditions of power plants profitability on spot markets. Energy Convers Manag 2019;198. https://doi.org/10.1016/j.enconman.2018.11.082.
[53] Rovira A, Montes MJ, Varela F, Gil M. Comparison of Heat Transfer Fluid and Direct Steam Generation technologies for Integrated Solar Combined Cycles. Appl Therm Eng 2013;52:264–74. https://doi.org/10.1016/j.applthermaleng.2012.12.008.
[54] Martín M, Sánchez D. A detailed techno-economic analysis of gas turbines applied to concentrated solar power plants with central receiver. J Eng Gas Turbines Power 2019;141:1–11. https://doi.org/10.1115/1.4040844.
[55] Bravo R, Ortiz C, Chacartegui R, Friedrich D. Multi-objective optimisation and guidelines for the design of dispatchable hybrid solar power plants with thermochemical energy storage. Appl Energy 2021;282:116257. https://doi.org/10.1016/j.apenergy.2020.116257.

[56] Bailera M, Pascual S, Lisbona P, Romeo LM. Modelling calcium looping at industrial scale for energy storage in concentrating solar power plants. Energy 2021;225:120306. https://doi.org/10.1016/j.energy.2021.120306.